Available online at www.sciencedirect.com
SCIENCE DIRECT®
Journal of Solid State Chemistry 177 (2004) 875–882
JOURNAL OF SOLID STATE CHEMISTRY
http://elsevier.com/locate/jssc

Luminescent and structural properties of the series $Ba_{6-x}Eu_xTi_{2+x}Ta_{8-x}O_{30}$ and $Ba_{4-y}K_yEu_2Ti_{4-y}Ta_{6+y}O_{30}$

Guobao Li,* Lei Cheng, Fuhui Liao, Shujian Tian, Xiping Jing, and Jianhua Lin

State Key Laboratory of Rare Earth Materials Chemistry and Applications, College of Chemistry and Molecular Engineering, Peking University, Chenfu Road 202, Beijing 100871, People's Republic of China

Received 4 July 2003; received in revised form 19 September 2003; accepted 24 September 2003

Abstract

The series $Ba_{6-x}Eu_xTi_{2+x}Ta_{8-x}O_{30}$ and $Ba_{4-y}K_yEu_2Ti_{4-y}Ta_{6+y}O_{30}$ have been synthesized at 1400°C in air. They exhibit efficient excitation at about 400 nm and typical emission of Eu^{3+} at about 580–620 nm, form solid solutions within $0.0 \leqslant x \leqslant 2.0$ and $0 \leqslant y \leqslant 4$ respectively, and crystallized in $P4/mbm$ at room temperature with Eu atoms occupied at centrosymmetric site (0, 0, 0). Their conductivity is very low ($2.8 \times 10^{-6}\,\Omega^{-1}\,cm^{-1}$ at 740°C for $Ba_6Ti_2Ta_8O_{30}$).

Keywords: Luminescence; Tetragonal tungsten-bronze

1. Introduction

Tungsten-bronze (TB) is a common structure type adopted by many different compounds with a general formula A_xMO_3 ($0 \leqslant x \leqslant 1$) [1–6]. The basic frameworks of TB are composed of corner-sharing MO_6 octahedra that are connected to form 3-, 4-, 5- and/or 6-octahedral rings in which A-type atoms are located. Four different tungsten bronze structure types have been known so far, i.e., perovskite tungsten bronze [7,8], tetragonal tungsten bronze (TTB) [9], hexagonal tungsten bronze [10], and intergrowth tungsten bronze [11]. In these compounds, the A-type atoms are varieties of alkaline or alkaline earth elements, such as Li, K, Na, Ba, Sr, etc., while octahedral sites are those transition metal cations with high valence, such as W, Ta, Nb, Ti, Zr. In general, these materials are interested due to their wide varieties of physical properties, such as electro-optical [12], nonlinear optical [13], pyroelectric [14], and acoustic property [15] and so on. As a mater of fact, the luminescent property of such materials might also be interesting [16] because there are considerable concerns of using the heavy transition metal compounds as the radioluminescent materials [17]. On the other hand, recent study also showed that, e.g., $Eu_{0.53}K_{2.41}Nb_6O_{17}$ with NbO_6 octahedra [18], have strong absorption at about 394 nm which might be useful in white light-emitting-diode devices [19–25] where a phosphor with a strong excitation/absorption around 394 nm is helpful. Therefore, the luminescent property of tungsten bronze structure compounds with corner-sharing MO_6 octahedra (M = Ta, Nb, etc.) may be very interesting. Here in this report, we present structural and luminescent properties of the Eu doped, Eu and K co-doped $Ba_6Ti_2Ta_8O_{30}$. These materials crystallize in TTB structure and exhibit efficient excitation at about 400 nm and typical emission of Eu^{3+} at about 580–620 nm.

2. Experimental

The Eu and K doped $Ba_6Ti_2Ta_8O_{30}$ materials were synthesized by high-temperature solid-state reaction using stoichiometric $BaCO_3$ (A.R.), K_2CO_3 (A.R.), Eu_2O_3 (99.99%), Ta_2O_5 (99.99%) and TiO_2 (A.R.) as the starting materials. The doped Eu^{3+} and K^+ occupied presumably the Ba positions in the structure; thus simultaneous adjustment of Ta^{5+} and Ti^{4+} is needed in order to compensate the extra charge. A series of samples with a general formula $Ba_{6-x}Eu_xTi_{2+x}Ta_{8-x}O_{30}$ and $Ba_{4-y}K_yEu_2Ti_{4-y}Ta_{6+y}O_{30}$, where

*Corresponding author. Fax: +861062751708.
E-mail address: gbli@chem.pku.edu.cn (G. Li).

0022-4596/$ - see front matter © 2003 Elsevier Inc. All rights reserved.
doi:10.1016/j.jssc.2003.09.023

the x and y varied from 0.0 to 4.00, have been synthesized as follows. The oven-dried starting materials of total about 6.0 g were mixed and ground. The mixtures were initially calcinated at 1200°C for 10 h. After that, they were heated at 1400°C in air for 10 h and then reground and heated until the X-ray diffraction patterns of the products did not change. During the reaction, the samples were also weighted to monitor the possible loss of the components. The maximum loss was about 4 mg for 6.0 g samples. Therefore, the composition of the sample was thought to be the weighted composition initially.

X-ray diffraction data were collected by using XRD-6000 diffractometer employing Cu$K\alpha$ radiation ($\lambda_{CuK\alpha1} = 1.54056$l Å, $\lambda_{CuK\alpha2} = 1.54440$ Å) with a Ni filter, a slits setting of 1/2, 1/2, 0.3, and 40 kV, 40 mA in a continuous scanning mode (2θ from 7° to 120°, 0.15°/min). X-ray diffraction data were analyzed by Rietveld refinement using GSAS [26]. The excitation and emission spectra were recorded with a Hitachi F-4500 fluorescence spectrophotometer. UV absorption spectra were recorded on an UV-3100 UV–VIS–NIR spectrophotometer using $BaSO_4$ as the reference. AC impedance data were measured with a HP4192A impedance analyzer with a typical ac voltage of 50 mV. The frequency ranges from 5 Hz to 12 MHz and, temperature of measurement varies from 200°C to 800°C. Sample for AC impedance measurements were pressed into pellets under 10 MPa, which were sintered at 1400°C for 12 h. The typical size of pellets was about 13 mm in diameter and 3 mm in thickness with the relative density of about 92%. The pellets were pasted with Pt paste and heated at 800°C for 30 min.

3. Results and discussions

The series $Ba_{6-x}Eu_xTi_{2+x}Ta_{8-x}O_{30}$ and $Ba_{4-y}K_yEu_2Ti_{4-y}Ta_{6+y}O_{30}$ show interesting luminescent properties. Their excitation spectra are very similar as shown in Fig. 1, which is for $Ba_4Eu_2Ti_4Ta_6O_{30}$. There are two different excitation transitions. The sharp peaks from 360 to 480 nm originate from transitions with the f-configuration from $^7F_0$ to excited states [27]. While the broadband around 330 nm may attribute to the transition from valence band, which is mainly the O 2p orbitals, to the conduction band, which is composed of mainly the d orbitals of the transition metals. Interestingly, the charge transfer transition of O^{2-}–Eu^{3+}, which normally appears at about 250 nm, is not present for these materials. Actually similar phenomenon was observed for another solid $K_{13}Eu(SiW_{11}O_{39})_2$ [28], where charge transfer band is also very weak.

To understand this phenomenon, UV absorption spectra have been measured as shown in Fig. 2. All the samples, including the undoped $Ba_6Ti_2Ta_8O_{30}$, show

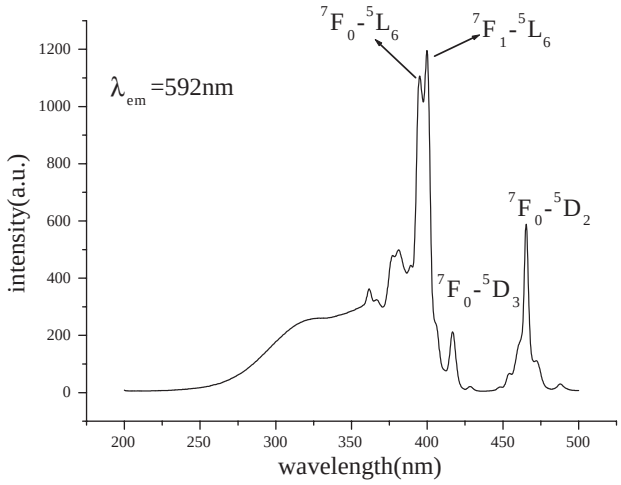

Fig. 1. Typical excitation spectra of the TTB $Ba_{6-x}Eu_xTi_{2+x}Ta_{8-x}O_{30}$ ($0 \leqslant x \leqslant 2.0$) monitored at 592 nm with $x = 2.00$.

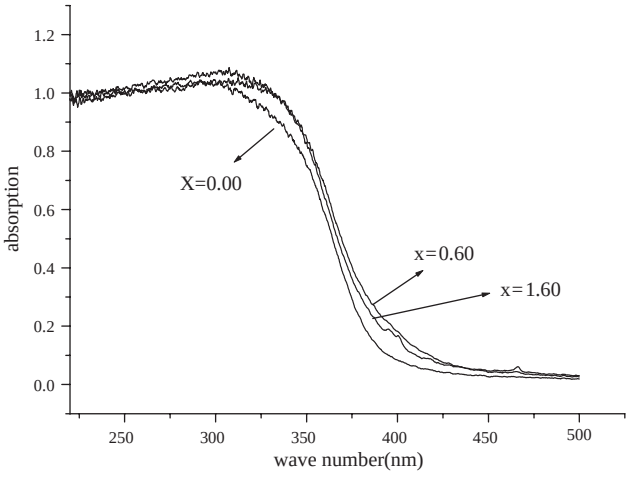

Fig. 2. UV absorption spectra of TTB $Ba_{6-x}Eu_xTi_{2+x}Ta_{8-x}O_{30}$ ($0 \leqslant x \leqslant 2.0$) with $x = 0.00$, 0.60, and 1.60.

similar absorption band covering most of UV range up to 330 nm. This strong absorption is attributed to the transition from valence band to conduction band. The band gap of the materials is usually estimated from the spectra according to the following equation:

$$E_{gap} = \frac{hC}{\lambda}. \quad (1)$$

Here h is the Plank constant, C the speed of light in vacuum, and λ is the wavelength corresponding to half maximum of the absorption band, which is about 350 nm for these materials. Taking all these parameters into account, the estimated band gap is about 3.5 eV, which is far smaller than the energy difference between the O-2p and Eu-4f. In such cases, therefore, the charge transfer transition of O^{2-}–Eu^{3+} is quenched in these narrow band materials.

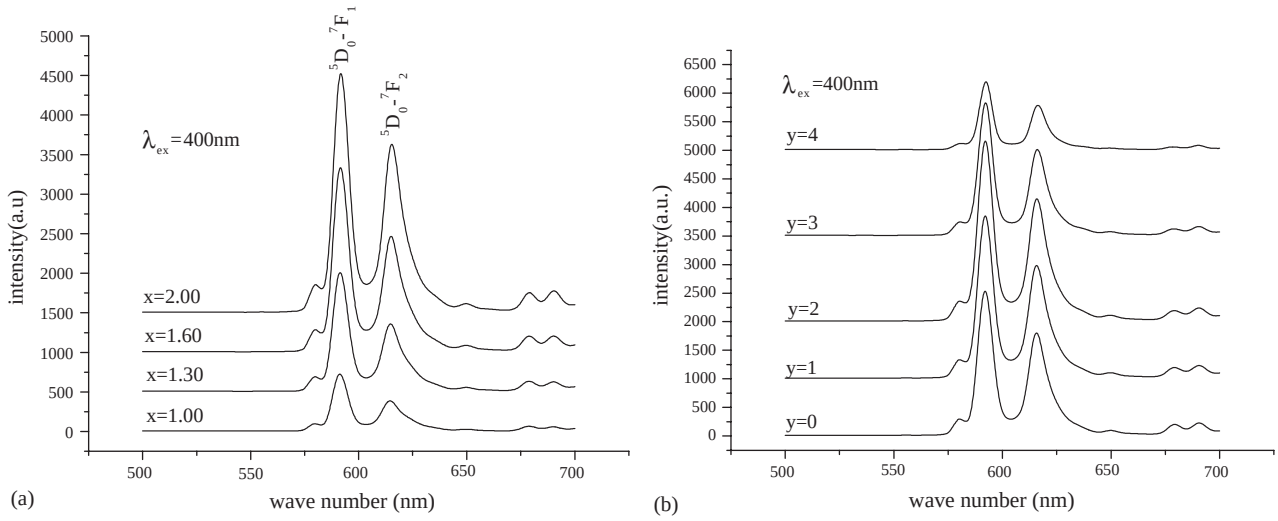

Fig. 3. Emission spectra of the series $Ba_{6-x}Eu_xTi_{2+x}Ta_{8-x}O_{30}$ and $Ba_{4-y}K_yEu_2Ti_{4-y}Ta_{6+y}O_{30}$ under 400 nm excitation: (a) $Ba_{6-x}Eu_xTi_{2+x}Ta_{8-x}O_{30}$ with $x = 1.00$, 1.30, 1.60 and 2.00; and (b) $Ba_{4-y}K_yEu_2Ti_{4-y}Ta_{6+y}O_{30}$ with $y = 0.00$, 1.00, 2.00, 3.00 and 4.00.

The Eu^{3+} doped materials $Ba_{6-x}Eu_xTi_{2+x}Ta_{8-x}O_{30}$ and $Ba_{4-y}K_yEu_2Ti_{4-y}Ta_{6+y}O_{30}$ exhibit orange red emission as shown in Fig. 3. The spectra are dominant by two transitions, $^5D_0 \rightarrow {}^7F_1$ (592 nm) and $^5D_0 \rightarrow {}^7F_2$ (611 nm). It is well known that $^5D_0 \rightarrow {}^7F_1$ is magnetic dipole transition in nature and is independent of the crystallographic site of the Eu^{3+} ions. $^5D_0 \rightarrow {}^7F_2$ is electric dipole transition implying Eu^{3+} ions occupied the noncentrosymmetric sites. However, thermal vibration of the atoms in centrosymmetric sites also make the atoms look like that occupying noncentrosymmetric sites. Therefore, the present observations shown in Fig. 3 just means that some or all of Eu atoms distribute in centrosymmetric sites and that the distribution of Eu atoms in two series is the same (the shape and intensity ratio of $^5D_0 \rightarrow {}^7F_1$ to $^5D_0 \rightarrow {}^7F_2$ were same). This implies that Eu atoms might mainly occupy the centrosymmetric site or then they are randomly distributed in both centrosymmetric and noncentrosymmetric sites. In order to have a clear answer, the structures of the series $Ba_{6-x}Eu_xTi_{2+x}Ta_{8-x}O_{30}$ and $Ba_{4-y}K_yEu_2Ti_{4-y}Ta_{6+y}O_{30}$ were carefully studied.

Two space groups $P4/mbm$ and $P4bm$ were found to fit the powder X-ray diffraction patterns of the $Ba_6Ti_2Ta_8O_{30}$ very well, as shown in Fig. 4. The details of the refinements are listed in Table 1. However, Zhang et al. [29] reported that the $Ba_6Ti_2Ta_8O_{30}$ is paraelectric at room temperature with a Curie temperature of about −35°C. Therefore, it is obvious that $Ba_6Ti_2Ta_8O_{30}$ crystallize in the space group $P4/mbm$ above −35°C, which might reduce to $P4bm$ below this temperature. This result is comparable to the reduced $Ba_6Ta_{10}O_{30}$ [30], which also crystallizes in $P4/mbm$.

In general, the TTB structure can be expressed as $(A1)_4(A2)_2(A3)_4(M1)_2(M2)_8O_{30}$ [31]. As shown in Fig. 5, there are two octahedral sites, i.e., $M1$ and $M2$, which in this compound are occupied randomly by Ti and Ta; the three different A-type positions can be either vacant or accommodated by large cations. In $Ba_6Ti_2Ta_8O_{30}$ barium atoms occupied two of the A-sites ($A1$ and $A2$), while the $A3$ are vacant. For the europium doped series $Ba_{6-x}Eu_xTi_{2+x}Ta_{8-x}O_{30}$ and $Ba_{4-y}K_yEu_2Ti_{4-y}Ta_{6+y}O_{30}$, the dopant atoms Eu and K substitute Ba at the A-type positions, meanwhile Ta and Ti is adjusted, thus to compensate the extra charge induced by Eu^{3+} and K^+. The Rietveld refinements confirm that they crystallize in TTB structure as that of $Ba_6Ti_2Ta_8O_{30}$.

In Figs. 6 and 7, the typical powder X-ray diffraction patterns for the series $Ba_{6-x}Eu_xTi_{2+x}Ta_{8-x}O_{30}$ and $Ba_{4-y}K_yEu_2Ti_{4-y}Ta_{6+y}O_{30}$ have been shown. It is found that single-phase products can be obtained up to $x = 2.00$ for $Ba_{6-x}Eu_xTi_{2+x}Ta_{8-x}O_{30}$ and up to $y = 4.00$ for $Ba_{4-y}K_yEu_2Ti_{4-y}Ta_{6+y}O_{30}$. These are further confirmed by the variation of the lattice parameters with the Eu or K content, as shown in Figs. 8 and 9 (the corresponding details are listed in Tables 2 and 3). For the series $Ba_{6-x}Eu_xTi_{2+x}Ta_{8-x}O_{30}$, both lattice parameters a and c decrease with the increase of the Eu content mainly caused by the fact that the radii of Eu^{3+} and Ti^{4+} were smaller than that of Ba^{2+} and Ta^{5+} [32]. As for the series $Ba_{4-y}K_yEu_2Ti_{4-y}Ta_{6+y}O_{30}$, lattice parameter a increased and c decreased with the increase of the K content. These changes agree nicely with the Vegard's law [33,34]. The corresponding solid solution limits are then suggested to be $0.0 \leqslant x \leqslant 2.0$ for the TTB $Ba_{6-x}Eu_xTi_{2+x}Ta_{8-x}O_{30}$ and $0.0 \leqslant y \leqslant 4.0$ for $Ba_{4-y}K_yEu_2Ti_{4-y}Ta_{6+y}O_{30}$.

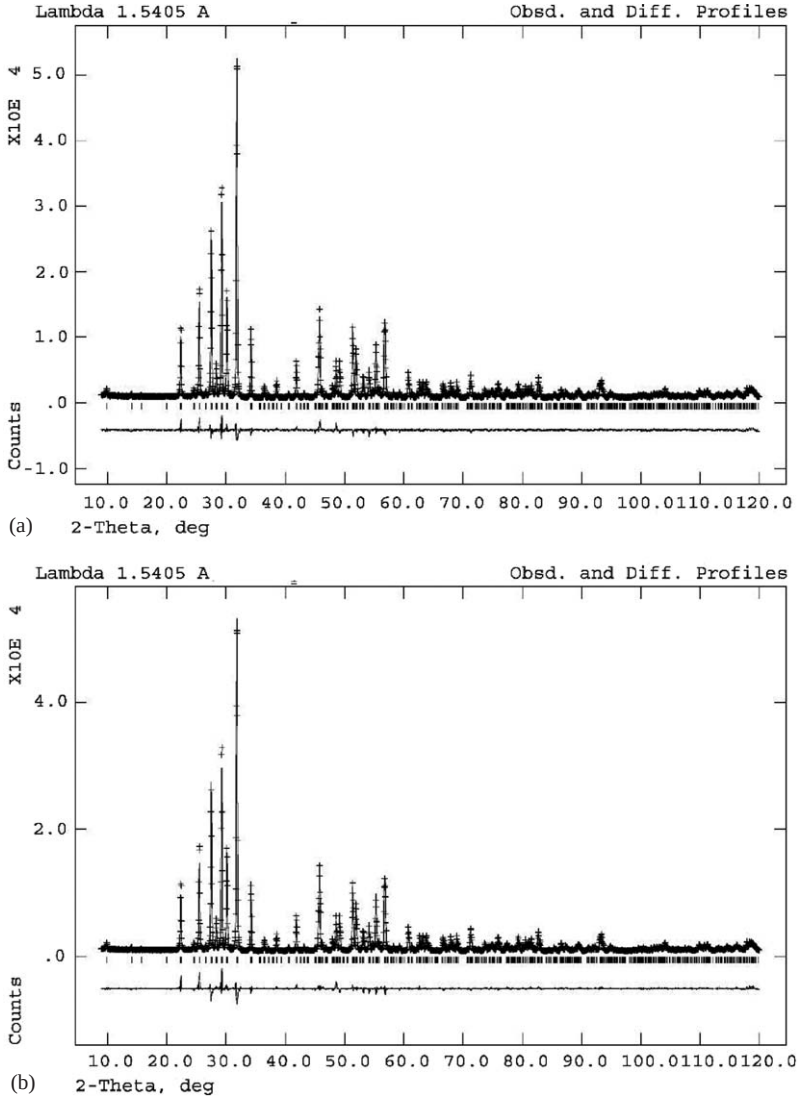

Fig. 4. The Rietveld plot of the powder X-ray diffraction patterns of the sample $Ba_6Ti_2Ta_8O_{30}$ with the different models. (a) *P*4/*mbm*; and (b) *P*4*bm*.

Table 1
Comparison of the different models for $Ba_6Ti_2Ta_8O_{30}$

Space group	*P*4/*mbm*[a]	*P*4*bm*[b]
a (Å)	12.5705(1)	12.5705(1)
c (Å)	3.9581(1)	3.9581(1)
Ba1 2a	0, 0, 0	0, 0, 0[c]
Ba2 4g	0.1718(1), 0.6718(1), 0	0.1720(1), 0.6720(1), −0.0002(1)
Ta/Ti1	0, 1/2, 1/2	0, 1/2, 0.4898(1)
Ta/Ti2	0.0744(1), 0.2146(1), 1/2	0.0744(1), 0.2147(1), 0.5003(1)
O1	0, 1/2, 0	0, 1/2, 0.0198(1)
O2	0.2830(1), 0.7830(1), 1/2	0.2830(1), 0.7830(1), 0.4982(1)
O3	0.0750(1), 0.2070(1), 0	0.0754(1), 0.2076(1), 0.0331(1)
O4	0.3415(1), 0.0073(1), 1/2	0.3418(1), 0.0072(1), 0.5045(1)
O5	0.1393(1), 0.0706(1), 1/2	0.1399(1), 0.0711(1), 0.5125(1)
R	$R_{wp} = 0.056, R_p = 0.042$	$R_{wp} = 0.056, R_p = 0.042$
Reduced CHI**2	5.2	5.2

[a] Two crystallography parameters and 14 atomic parameters have been refined.
[b] Two crystallography parameters and 20 atomic parameters have been refined.
[c] The Ba1 atom is chosen as the origin in this space group.

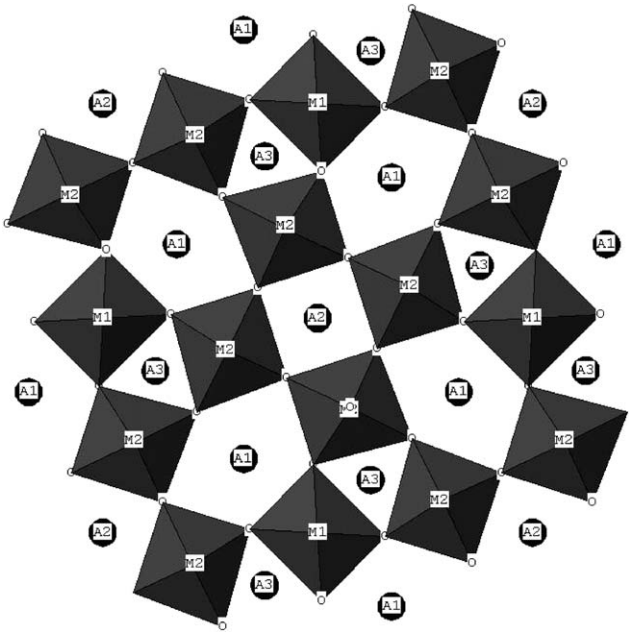

Fig. 5. The projection along c-axis of the TTB structure with the formula $(A1)_4(A2)_2(A3)_4(M1)_2(M2)_8O_{30}$.

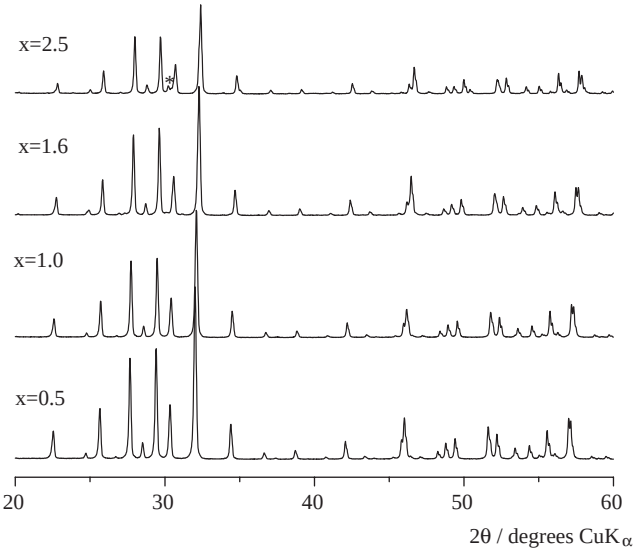

Fig. 6. Typical powder X-ray diffraction patterns of the series $Ba_{6-x}Eu_xTi_{2+x}Ta_{8-x}O_{30}$ $(0\leqslant x\leqslant 4.0)$ * is of unknown phase.

As mentioned above, the distribution of Eu atoms are the same in these two series $Ba_{6-x}Eu_xTi_{2+x}Ta_{8-x}O_{30}$ and $Ba_{4-y}K_yEu_2Ti_{4-y}Ta_{6+y}O_{30}$. There are two cases, one is that all of Eu atoms occupy the $A2$ site (centrosymmetric site), the other was some of Eu atoms occupied $A2$ site and some in $A1$ site (noncentrosymmetric site). To make a choice, the refine profiles are compared in Fig. 10 for X-ray diffraction patterns of

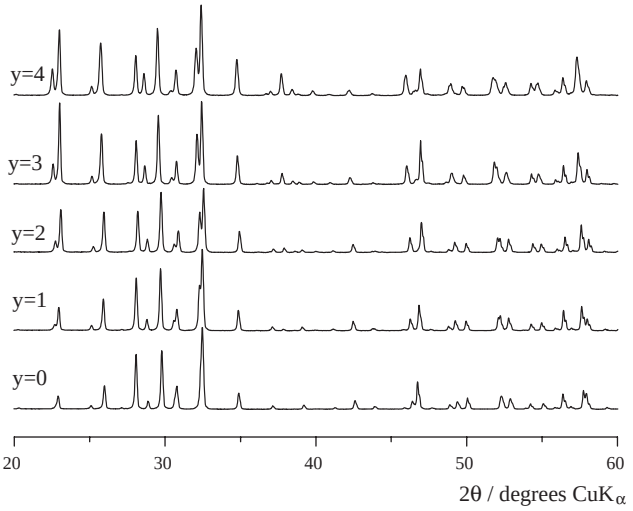

Fig. 7. Typical X-ray powder diffraction patterns of the series $Ba_{4-y}K_yEu_2Ti_{4-y}Ta_{6+y}O_{30}$ $(0\leqslant y\leqslant 4.0)$.

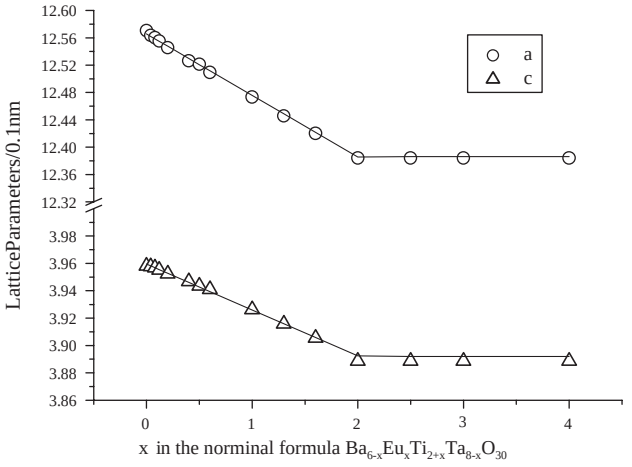

Fig. 8. Lattice parameters of the tetragonal bronze $Ba_{6-x}Eu_xTi_{2+x}Ta_{8-x}O_{30}$ phase in the different samples.

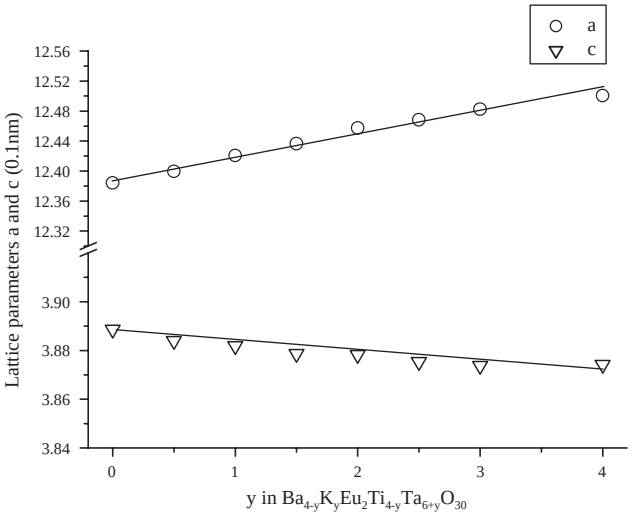

Fig. 9. Lattice parameters of the tetragonal bronze $Ba_{6-x}Eu_xTi_{2+x}Ta_{8-x}O_{30}$ phase in the different samples.

$Ba_4Eu_2Ti_4Ta_6O_{30}$ with all Eu atoms at $A2$ site, and 1/3 at $A2$ and 2/3 at $A1$ site, respectively. The corresponding refinement details are listed in Table 4. It is clear that no obvious differences are observed. The main reason might be that the X-ray diffraction ability of Ba and Eu atoms is almost the same. Because the X-ray diffraction ability of K and Eu is very different, similar comparison shown in Fig. 11 induces that Eu atoms should occupy mainly $A2$ site for the other case gave a very bad fitting of the X-ray diffraction patterns. The corresponding refinement details are listed in Table 5.

Table 2
Lattice parameters of the tetragonal tungsten bronze phase in the sample with the nominal formula $Ba_{6-x}Eu_xTi_{2+x}Ta_{8-x}O_{30}$ $(0.00 \leqslant x \leqslant 4.00)$

x	a (Å)	c (Å)	V (Å^3)
0.00	12.5705(1)	3.9582(1)	625.45(1)
0.04	12.5636(1)	3.9578(1)	624.71(1)
0.08	12.5602(1)	3.9568(1)	624.21(1)
0.12	12.5553(1)	3.9551(1)	623.48(1)
0.20	12.5456(1)	3.9524(1)	622.08(1)
0.40	12.5264(1)	3.9467(1)	619.29(1)
0.50	12.5213(1)	3.9434(1)	618.26(1)
0.60	12.5094(1)	3.9410(1)	616.71(1)
1.0	12.4732(1)	3.9263(1)	610.85(1)
1.30	12.4457(1)	3.9159(1)	606.55(1)
1.60	12.4201(1)	3.9054(1)	602.45(1)
2.00	12.3842(1)	3.8886(1)	596.38(1)
2.50	12.3842(1)	3.8886(1)	596.38(1)
3.00	12.3842(1)	3.8886(1)	596.38(1)
4.00	12.3842(1)	3.8886(1)	596.38(1)

Table 3
Lattice parameters of the tetragonal tungsten bronze phase in the sample with the nominal formula $Ba_{4-y}K_yEu_2Ti_{4-y}Ta_{6+y}O_{30}$ $(0.00 \leqslant y \leqslant 4.00)$

y	a (Å)	c (Å)	V (Å^3)
0.00	12.3842(1)	3.8886(1)	596.38(1)
0.50	12.3995(1)	3.8840(1)	597.16(1)
1.00	12.4207(1)	3.8819(1)	598.87(1)
1.50	12.4366(1)	3.8787(1)	599.91(1)
2.00	12.4573(1)	3.8783(1)	601.84(1)
2.50	12.4684(1)	3.8754(1)	602.47(1)
3.00	12.4824(1)	3.8738(1)	603.57(1)
4.00	12.5006(1)	3.8742(1)	605.40(1)

The conductivity of these two series $Ba_{6-x}Eu_xTi_{2+x}Ta_{8-x}O_{30}$ $(0 \leqslant x \leqslant 2)$ and $Ba_{4-y}K_yEu_2Ti_{4-y}Ta_{6+y}O_{30}$ $(0 \leqslant y \leqslant 4)$ was measured by impedance spectra. Fig. 12 shows typical impedance spectrum for $Ba_5EuTi_3Ta_7O_{30}$ at 780°C. The semi-circle is associated to the contribution of impedance from bulk. The conductivity of all samples behaves rather similar and agrees well with Arrhenius' law as shown in Fig. 13.

$$\sigma T = A e^{-E_a/kT}. \quad (2)$$

Here, T is the temperature in Kelvins, σ the conductivity of the samples ($\Omega^{-1}\,cm^{-1}$), E_a the active energy, k the Boltzmann's constant. The activation energies are almost the same about 1.55 eV.

In conclusion, the europium substituted systems $Ba_{6-x}Eu_xTi_{2+x}Ta_{8-x}O_{30}$ and $Ba_{4-y}K_yEu_2Ti_{4-y}Ta_{6+y}O_{30}$, which have TTB structure, were obtained by high-temperature solid-state reaction at 1400°C. The main excitations of these materials originate from the $f-f$ and crossing-band transition, and the charge transfer of O^{2-}–Eu^{3+} does not appear. They form solid solution below $x = 2.0$ or $y = 4.0$. Eu atoms occupy mainly the centrosymmetric site in the lattice. The strong emission at 592 nm is caused by Eu^{3+} at the centrosymmetric site.

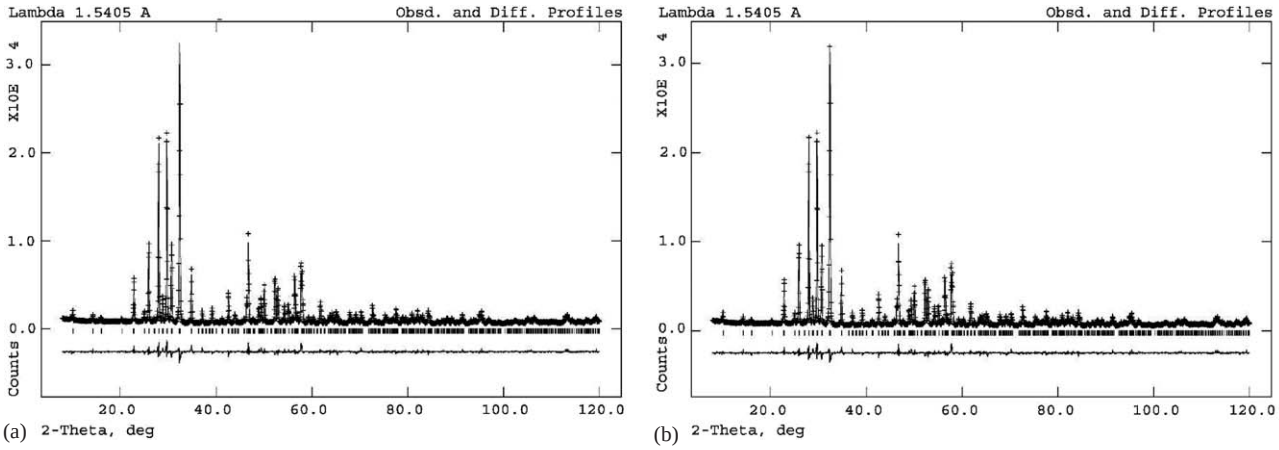

Fig. 10. The Rietveld plot of the powder X-ray diffraction patterns of the sample $Ba_4Eu_2Ti_4Ta_6O_{30}$ with the different models. (a) All of Eu atoms at the site 2a; and (b) 1/3 of Eu atoms at 2a and 2/3 of Eu atoms at 4g (reference to Table 1).

Table 4
Comparison of the different models[a] for $Ba_4Eu_2Ti_4Ta_6O_{30}$

Atom	Coordination	Occupation	
		Model a	Model b
Ba/Eu1 2a	0, 0, 0	0.00/1.00	0.666/0.333
Ba/Eu2 4g	0.1709(1), 0.6709(1), 0	1.00/0.00	0.666/0.333
Ta/Ti1	0, 1/2, 1/2	0.60/0.40	0.60/0.40
Ta/Ti2	0.0748(1), 0.2135(1), 1/2	0.60/0.40	0.60/0.40
O1	0, 1/2, 0	1.00	1.00
O2	0.2870(1), 0.7870(1), 1/2	1.00	1.00
O3	0.0742(1), 0.1950(1), 0	1.00	1.00
O4	0.3393(1), 0.0025(1), 1/2	1.00	1.00
O5	0.1366(1), 0.0637(1), 1/2	1.00	1.00
R values		$R_{wp} = 6.6\%$, $R_p = 4.9\%$	$R_{wp} = 6.6\%$, $R_p = 4.9\%$
Reduced CHI**2		6.1	6.1

[a] The basic crystallography parameters are the same: Space group $P4/mbm$ with $a = 12.3842(1)$ (Å), $c = 3.8886(1)$ (Å).

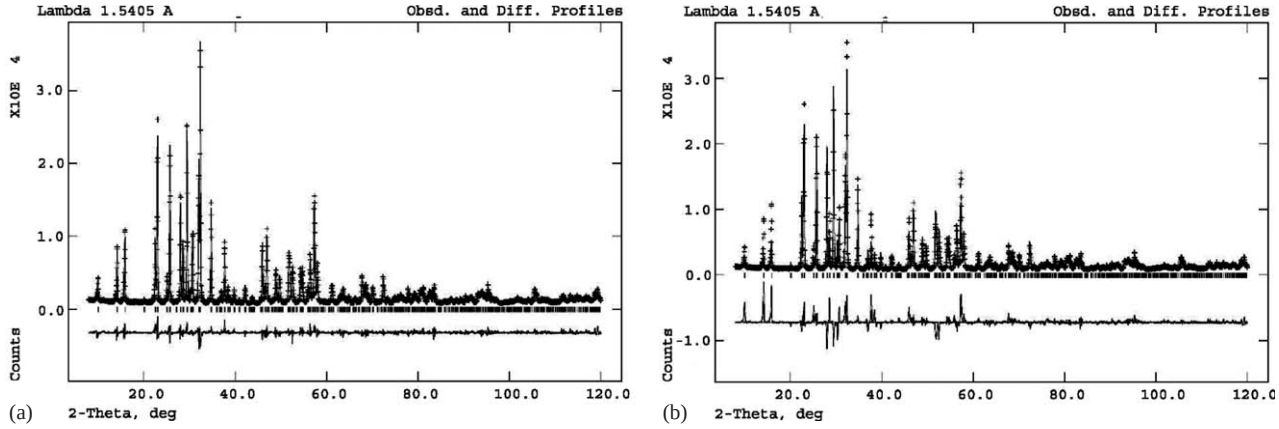

Fig. 11. The Rietveld plot of the powder X-ray diffraction patterns of the sample $K_4Eu_2Ta_{10}O_{30}$ with the different models. (a) All of Eu atoms at the site 2a; and (b) 1/3 of Eu atoms at 2a and 2/3 of Eu atoms at 4g (reference to Table 1).

Table 5
Comparison of the different models[a] for $K_4Eu_2Ta_{10}O_{30}$

Atom	Coordination	Occupation	
		Model a	Model b
K/Eu1 2a	0, 0, 0	0.00/1.00	0.666/0.333
K/Eu2 4g	0.1698(1), 0.6698(1), 0	1.00/0.00	0.666/0.333
Ta1	0, 1/2, 1/2	1.00	1.00
Ta2	0.0758(1), 0.2140(1), 1/2	1.00	1.00
O1	0, 1/2, 0	1.00	1.00
O2	0.2808(1), 0.7808(1), 1/2	1.00	1.00
O3	0.0735(1), 0.1979(1), 0	1.00	1.00
O4	0.3463(1), 0.0051(1), 1/2	1.00	1.00
O5	0.1395(1), 0.0633(1), 1/2	1.00	1.00
R-values		$R_{wp} = 8.0\%$, $R_p = 6.0\%$	$R_{wp} = 16.7\%$, $R_p = 11.8\%$
Reduced CHI**2		11.9	52.2

[a] The basic crystallography parameters are the same: space group $P4/mbm$ with $a = 12.5006(1)$ (Å), $c = 3.8742(1)$ (Å).

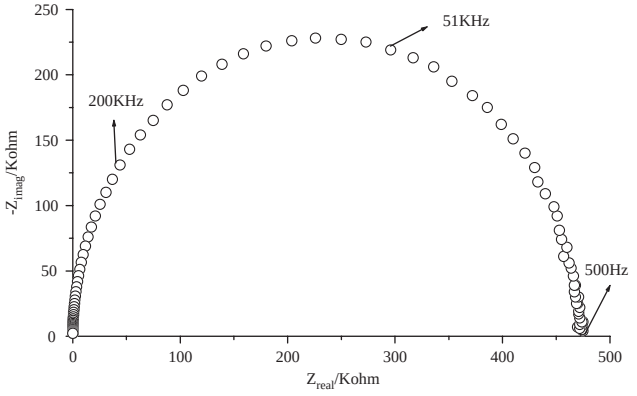

Fig. 12. Impedance spectra of the sample $Ba_{6-x}Eu_xTi_{2+x}Ta_{8-x}O_{30}$ with $x = 1.00$ at 780°C.

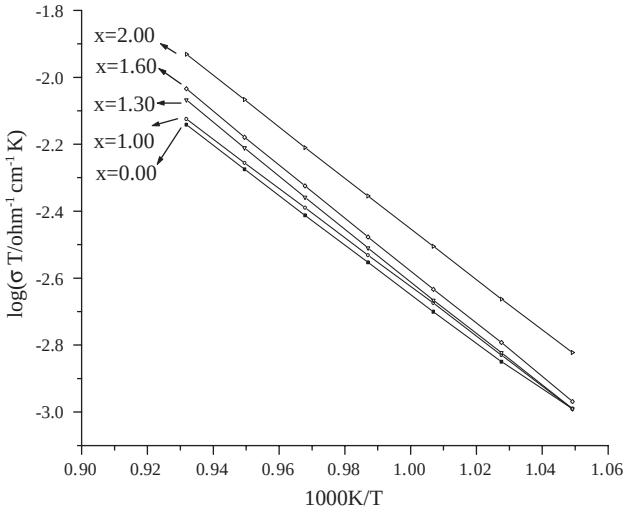

Fig. 13. Typical conductivity of the series $Ba_{6-x}Eu_xTi_{2+x}Ta_{8-x}O_{30}$ ($0 \leqslant x \leqslant 2.0$) at different temperatures.

Acknowledgments

The authors are thankful to the financial support from NSFC and State Key Basic Research Program of China.

References

[1] L. Bartha, A.B. Kiss, T. Szalay, Int. J. Refractory Metals Hard Mater. 13 (1995) 77–91.
[2] R.D.J. Tilley, Int. J. Refractory Metals Hard Mater. 13 (1995) 93–109.
[3] Ph. Labbe, H. Leligny, B. Raveau, J. Schneck, J.C. Toledano, J. Phys.: Condens. Matter 2 (1990) 25–43.
[4] K. Dusek, J. Ludecke, S. van Smaalen, J. Mater. Chem. 12 (2002) 1408–1414.
[5] P. Roussel, O. Perez, P. Labbe, Acta Crystallogr. B 57 (2001) 603–632.
[6] G.K. Zhang, L.Q. Qin, J.G. Yu, J. Wuhan Univ. Technol. 15 (2000) 57–60.
[7] C. Grenthe, M. Sundberg, J. Solid State Chem. 167 (2002) 412–419.
[8] V.P. Filonenko, C. Grenthe, M. Nygren, M. Sundberg, I.P. Zibrov, J. Solid State Chem. 163 (2002) 84–92.
[9] H. El Alaoui-Beighiti, A. Simon, M. Elaatmani, J.M. Reau, J. Ravez, Phys. Stat. Sol. (a) 187 (2001) 549–556.
[10] A. Hussain, A. Ul-Monir, M.M. Murshed, C.H. Rüscher, A. Anorg. Allg. Chem. 628 (2002) 416–420.
[11] L. Kihlborg, H. Blomqvist, M. Sundberg, J. Solid State Chem. 162 (2001) 341–346.
[12] O. Eknoyan, H.F. Taylor, J.M. Marx, Z. Tang, R.R. Neurgaonkar, Ferroelectrics 205 (1998) 147–158.
[13] T. Karaki, K. Miyashita, M. Nakatsuji, M. Adachi, Jpn. J. Appl. Phys. Part 1 37 (1998) 5277–5279.
[14] I.A. Santos, D. Garcia, J.A. Eiras, Ferroelectrics 257 (2001) 105–110.
[15] I.G. Siny, S.G. Lushnikov, S.I. Siny, V.H. Schmidt, A.A. Savvinov, R.S. Katiyar, J. Appl. Phys. 89 (2001) 1671–1678.
[16] A.A. Kaminskii, V.A. Koptsik, Yu.A. Maskaev, I.I. Naumova, L.N. Rashkovich, S.E. Sarkisov, Phys. Stat. Sol. A 28 (1975) K5–K10.
[17] B. Li, Z.N. Gu, J.H. Lin, M.Z. Su, Mater. Res. Bull. 35 (2000) 1921–1931.
[18] V.R.L. Constantino, M.A. Bizeto, H.F. Brito, J. Alloys Comp. 278 (1998) 142–148.
[19] S. Nakamura, T. Mukai, M. Senoh, Appl. Phys. Lett. 64 (1994) 1687.
[20] S. Nakamura, T. Mukai, M. Senoh, N. Iwasa, J. Appl. Phys. 76 (1994) 8189.
[21] S. Nakamura, M. Senoh, N. Iwasa, S. Nagahama, T. Yamada, T. Mukai, Jpn. J. Appl. Phys. 34 (1995) L1332.
[22] T. Mukai, D. Morita, S. Nakamura, J. Crystal Growth 189/190 (1998) 778.
[23] T. Mukai, M. Yamada, S. Nakamura, Jpn. J. Appl. Phys. 37 (1998) L1358.
[24] T. Mukai, H. Narimatsu, S. Nakamura, Jpn. J. Appl. Phys. 37 (1998) L479.
[25] Y. Narukawa, I. Niki, K. Izuno, M. Yamada, Y. Murazaki, T. Mukai, Jpn. J. Appl. Phys. 41 (2002) L371.
[26] A.C. Larson, R.B. von Dreele, report LAUR 86-748, Los Alamos National Laboratory, 1985.
[27] O. Visser, L. Visscher, P.J.C. Aerts, W.C. Nieuwpoort, J. Chem. Phys. 96 (1992) 2910.
[28] J. Wang, H.S. Wang, L.S. Fu, F.Y. Liu, H.J. Zhang, Thin Solid Films 414 (2002) 256–261.
[29] H. Zhang, L. Fang, R.Z. Yuan, Acta Phys. Chim. Sin. 17 (2001) 747–749.
[30] C.R. Feger, R.P. Ziebarth, Chem. Mater. 7 (1995) 373–378.
[31] P.B. Jamieson, S.C. Abrahams, J.L. Bernstein, J. Chem. Phys. 48 (1968) 5048.
[32] R.D. Shannon, Acta Crystallogr. A 32 (1976) 751.
[33] L. Vegard, Z. Phys. 5 (1921) 17.
[34] L. Vegard, Z. Kristallogr. 67 (1928) 239.